Journal of Molecular Structure 1326 (2025) 141045

Contents lists available at ScienceDirect

Journal of Molecular Structure

journal homepage: www.elsevier.com/locate/molstr

The electronic states of 2-chlorotoluene in the 4.0–10.8 eV photon energy range

P.A.S. Randi [a], S. Kumar [b,c], A. Souza Barbosa [a], U.S. Akther [b], N.C. Jones [d], S.V. Hoffmann [d], M.H.F. Bettega [a,*], P. Limão-Vieira [a,b,*]

[a] Departamento de Física, Universidade Federal do Paraná, Caixa Postal 19044 81531-980 Curitiba, Paraná, Brazil
[b] Atomic and Molecular Collisions Laboratory, CEFITEC, Department of Physics, NOVA School of Science and Technology, Universidade NOVA de Lisboa 2829-516 Caparica, Portugal
[c] Chemical Sciences Division, Lawrence Berkeley National Laboratory, One Cyclotron Road, Berkeley 94720, California, USA
[d] ISA, Department of Physics and Astronomy, Aarhus University, Ny Munkegade 120, DK-8000, Aarhus C, Denmark

ARTICLE INFO

Keywords:
2-chlorotoluene
Cross-sections
Theoretical calculations
Spectroscopy

ABSTRACT

Absolute cross-section values of 2-chlorotoluene are reported from vacuum ultraviolet photoabsorption measurements in the photon energy range 4.0–10.8 eV (310–115 nm), together with quantum chemical calculations. The nature of the electronic states is associated with transitions from the neutral ground state to valence, mixed valence-Rydberg and Rydberg orbitals. The fine structure in the photoabsorption bands has been mainly assigned to C–H stretching (CH_3), $\nu'_6(a')$, C–H in-plane bending, $\nu'_{16}(a')/\nu'_{17}(a')$, C–Cl stretching, $\nu'_{21}(a')$ and C–C in-plane bending $\nu'_{23}(a')$ modes. The measured absolute photoabsorption cross sections have also been used to estimate the photolysis lifetime of 2-chlorotoluene in the upper stratosphere, showing that solar photolysis can only be a relevant sink at altitudes above 23 km. We have also performed calculations at the TD-DFT level to obtain optimised geometries, excitation energies, oscillator strengths and potential energy curves for the lowest-lying electronic excited states. Special attention is given to state-selective vibrational excitation to obtain information on the internal conversion mechanisms governing the nuclear dynamics in the photoabsorption regions where C=C stretching, C–H in-plane bending and C–Cl/C–CH_3 stretching modes have been assigned. The results show a relevant internal conversion from Rydberg to valence character and vice-versa, dictating the nuclear dynamics of 2-chlorotoluene upon photon absorption.

1. Introduction

Chlorotoluenes have attracted the attention of the international scientific community for their role as precursors to other chemical compounds relevant in the chemical and pharmaceutical industries [1–3] (and references therein). 2-chlorotoluene (*ortho*-chlorotoluene) has been used in the production of synthetic rubber and dyes, also as an insecticide and bactericide, and due to its wide use is expected to be mainly released into the environment through different sewage streams [2]. It has been noted to be toxic to aquatic organisms due to its inert nature to chemical hydrolysis [2], while recent studies recommend tracking health risks of 2-chlorotolune exposure as a volatile organic compound [3]. In recent years we have been interested in investigating the electronic state spectroscopy of toluene [4] and fluorinated toluenes [5–8] and also to provide as accurate as possible information on absolute photoabsorption cross-section values relevant for atmospheric modelling [9]. In spite of the general effort to determine the impact of chlorotoluenes in the terrestrial atmosphere (physical and chemical processes), we note a deficiency in the assessment of their electronic states in the ultraviolet photon energy region. Currently, our motivation is based upon the urgent need to contribute worldwide with a comprehensive description of the molecular structure while assigning the nature of the lowest-lying electronic states of 2-chlorotoluene.

A literature survey reveals theoretical and experimental methods that have been used to investigate some of the molecular properties of 2-chlorotoluene. These include Penning ionisation electron spectroscopy [10,11], studies of its photodissociation into Cl and C_7H_7 fragments [12], infrared and Raman spectroscopy [13,14] and rate constants for its reactions with hydroxyl radicals [15,16]. Also relevant to the present work, experimental methods on resonant two-photon ionisation and

* Corresponding authors.
E-mail addresses: bettega@fisica.ufpr.br (M.H.F. Bettega), plimaovieira@fct.unl.pt (P. Limão-Vieira).

https://doi.org/10.1016/j.molstruc.2024.141045
Received 26 September 2024; Received in revised form 11 November 2024; Accepted 6 December 2024
Available online 15 December 2024

pulsed field ionisation [17] and calculations on the molecular geometry and the potential function of the methyl torsion [18]. Regarding ultraviolet photoabsorption spectra relevant to the present work, we are only aware of a previous investigation in the wavelength region from 172.2 nm up to 279.1 nm (4.4–7.2 eV) [19] although with no spectral assignments [20]. Thus, the present work is the most complete characterisation of 2-chlorotoluene to date, combining experimental and theoretical methods on the electronic state spectroscopy. Vacuum ultraviolet radiation has been provided from a synchrotron facility to perform photoabsorption measurements, whilst time dependent density functional theory (TD-DFT) calculations provide energies and oscillator strengths for the lowest-lying neutral states. Moreover, we have obtained with the TD-DFT method potential energy curves for the lowest-lying excited states as a function of the vibrational modes $\nu_7(a')$, $\nu_{17}(a')$ and $\nu_{21}(a')$. Finally, 2-chlorotoluene experimental absolute cross-section values have been used to estimate the molecule's lifetime in the Earth's atmosphere (from 0 up to 50 km altitude), while the detailed information about its electronically excited states can be used for modelling such chemical compounds in terrestrial environments.

2. Experimental method

The AU-UV beam line of the ASTRID2 synchrotron facility at Aarhus University, Denmark was used to obtain vacuum ultraviolet (VUV) photoabsorption spectrum of 2-chlorotoluene in the photon energy range from 4.0 eV to 10.8 eV (Figs. 1–5). The different absorption features related to the electronic excitations have been assigned in Tables 1–6. The absorption gas cell end station where photoabsorption experiments were performed, has been described on previous occasions [21,22]. In short, synchrotron radiation passes through a static gas sample of 2-chlorotoluene vapour at room temperature with the transmitted light detected by a photomultiplier tube (PMT). The lower wavelength limit of detection (115 nm) is set by the MgF_2 transmission windows enclosing the cell. The absolute pressure of the sample in the absorption cell was measured by a capacitance manometer (Chell CDG100D), with the absorption cross-sections measured in the pressure range 0.02–1.29 mbar, to achieve attenuations of 50 % or less and hence avoid saturation effects.

The absolute photoabsorption cross-sections values, σ, in units of megabarn (1Mb $\equiv 10^{-18}$ cm^2) were obtained from the Beer-Lambert attenuation law: $I_t = I_0 e^{(-N\sigma l)}$, where I_t is the light intensity transmitted through the gas sample, I_o is that through the evacuated cell, N the molecular number density of 2-chlorotoluene, and l the absorption path length (15.5 cm). Throughout the collection of each spectrum, the synchrotron beam current was monitored, and background scans were recorded with the cell evacuated. Within the wavelength region scanned (115–310 nm), accurate cross-section values are obtained by recording the VUV spectrum in small (5 or 10 nm) sections, allowing an overlap of at least 10 points between the adjoining sections. ASTRID2 operates in a "top-up" mode allowing the light intensity to be kept quasi-constant, thus compensating for the constant beam decay in the storage ring. The variations (2–3 %) of the incident flux are therefore normalized to the beam current in the storage ring. This methodology allows us to determine photoabsorption cross-sections to an accuracy of ± 5 %. The resolution in the present spectrum is better than 0.08 nm [21], which corresponds to 1, 3, and 7 meV at the low extreme, the midpoint, and the high extreme of the photon energy range scanned, respectively.

The liquid sample used in the VUV photoabsorption measurements was purchased from Sigma-Aldrich, with a stated purity of 99 %. The sample was degassed through repeated freeze-pump-thaw cycles before use.

3. Theoretical methods

The calculations performed on the electronic structure and properties of the electronically excited states of 2-chlorotoluene have allowed the assignment of the different features in the photoabsorption spectrum. The optimised ground state geometry of 2-chlorotoluene is shown in Fig. S1 with bond lengths in Å and bond angles in (°). The vertical excitation energies and oscillator strengths of the most representative electronically excited states in Table 1 (see also Table S1), were calculated employing TD-DFT [23,24] with a B3LYP functional [25,26], and the aug-cc-pVDZ basis set as implemented in the GAMESS-US computational package [27]. Additional calculations have also been performed at the equation of motion coupled-cluster with single and double excitations (EOM-CCSD) level of theory [28–31], with the aug-cc-pVDZ basis set (Table S2) as implemented in Psi4 [32]. Furthermore, we have obtained harmonic frequencies (B3LYP/aug-cc-pVDZ) for the neutral electronic ground state (Table S3) and compared with experimental data available in the literature, ensuring the coordinates obtained from the geometry optimisation calculation are indeed the true potential minimum.

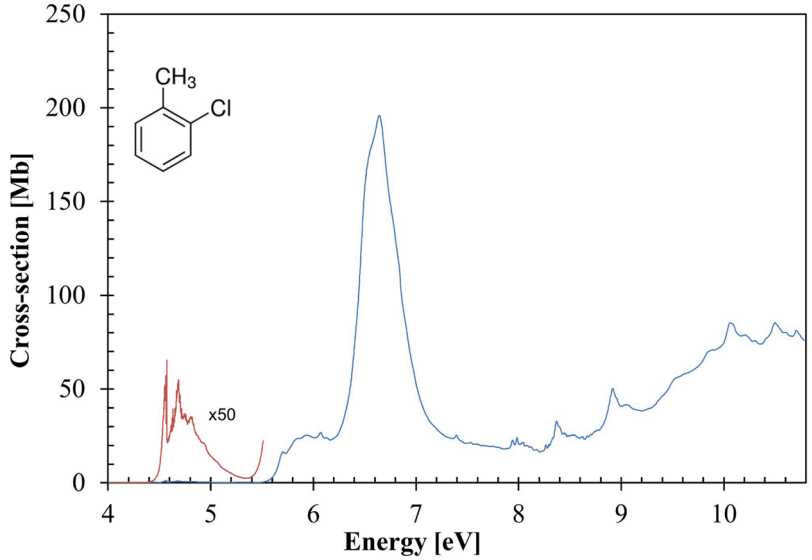

Fig. 1. The photoabsorption spectrum of 2-chlorotoluene in the 4.0–10.8 eV photon energy range. See text for details.

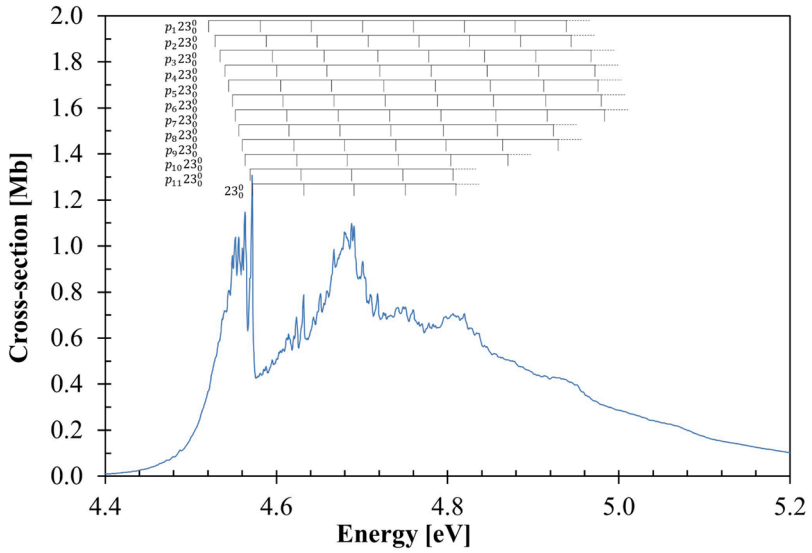

Fig. 2. Detail of the photoabsorption spectrum of 2-chlorotoluene in the 4.4–5.2 eV photon energy range. See text for details.

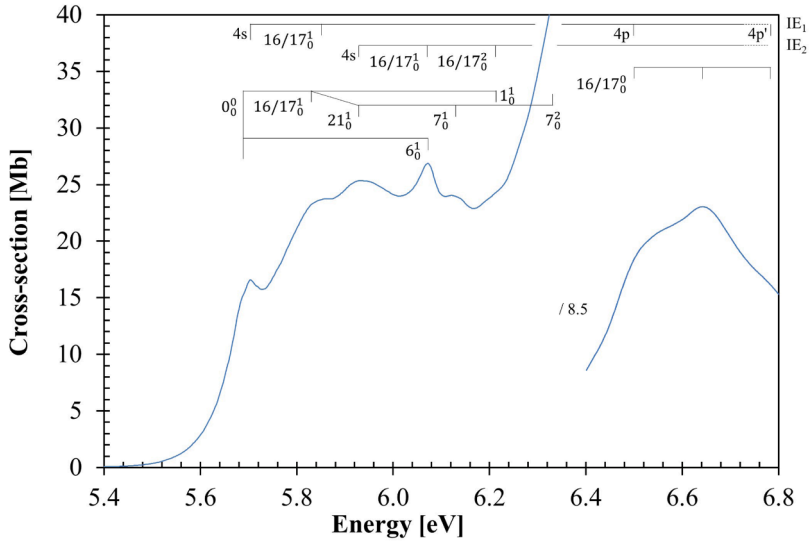

Fig. 3. Detail of the photoabsorption spectrum of 2-chlorotoluene in the 5.4–6.8 eV photon energy range with Rydberg series converging to $(6a'')^{-1}\ \widetilde{X}\ ^2A''$ (IE_1) and $(5a'')^{-1}\widetilde{A}\ ^2A''$ (IE_2). See text for details.

4. Structure and properties of 2-chlorotoluene

The neutral ground state and neutral first excited state geometries of 2-chlorotoluene obtained at the DFT and TD-DFT levels with the B3LYP/aug-cc-pVDZ basis set, together with their bond lengths (Å) and bond angles (°) are listed in the Supporting Material (Figs. S1 and S2). The calculated outermost electronic configuration of the $\widetilde{X}\ ^1A'$ ground state is … $(23a')^2\ (24a')^2\ (3a'')^2\ (25a')^2\ (26a')^2\ (4a'')^2\ (27a')^2\ (5a'')^2\ (6a'')^2$. A visual inspection of the ground state molecular orbitals (MOs) character (Fig. S3) shows the highest occupied molecular orbital (HOMO), 6a″, and the (HOMO-2), 27a', are Cl 3p lone pair orbitals (n_{Cl}) out-of-plane with ring π(C=C) characters. The second highest occupied molecular orbital (HOMO-1), 5a'', is π(C=C) with (n_{Cl}) out-of-plane, the (HOMO-2), 27a′, is ($\overline{n}_{Cl}$) in the molecular plane with σ_{CC} character, whereas (HOMO-3), 4a'', is (n_{Cl}) out-of-plane with π(C=C) character. Other MOs from which electrons can be excited are (HOMO-4), 26a′, and (HOMO-5), 25a′, both with $\sigma_{CC/Cl}$ character, while (HOMO-6), 3a″, and (HOMO-8), 23a′, are π(C=C) and $\sigma_{CC/CH}$ bonding. The major electronic excitation features in the VUV photoabsorption spectrum depicted in Figs. 1–5 have been assigned from these highest occupied molecular orbitals to valence, mixed valence-Rydberg and Rydberg character orbitals. The orbital character is determined from their spatial distribution (Fig. S3), and the electronically excited states are assigned based on the transitions that contribute most to their description. The calculated dominant excitation energies and oscillator strengths are listed in Table 1, while the complete set of calculated electronic transitions is in Table S1.

The fine structure visible in the photoabsorption spectrum is indicative of vibronic transitions in the valence, mixed valence-Rydberg and Rydberg transitions, with main vibrational modes assigned according to the experimental information from Raman and infrared spectroscopies [13,14], as well as from the harmonic frequencies calculations and labelling in Table S3. The main modes have been assigned based on the energies (and wavenumbers) in the neutral electronic ground state 0.355 eV (2860 cm^{-1}) for C–H stretching (CH_3), $\nu''_6(a')$, 0.144/0.140 eV (1158/1129 cm^{-1}) for C–H in-plane bending, $\nu''_{16}(a')/\nu''_{17}(a')$, 0.100 eV (804/805 cm^{-1}) for C–Cl stretching (C–CH_3 stretching and C–C in-plane bending), $\nu''_{21}(a')$ and 0.068/0.069 eV (552/554 cm^{-1}) for C–C in-plane

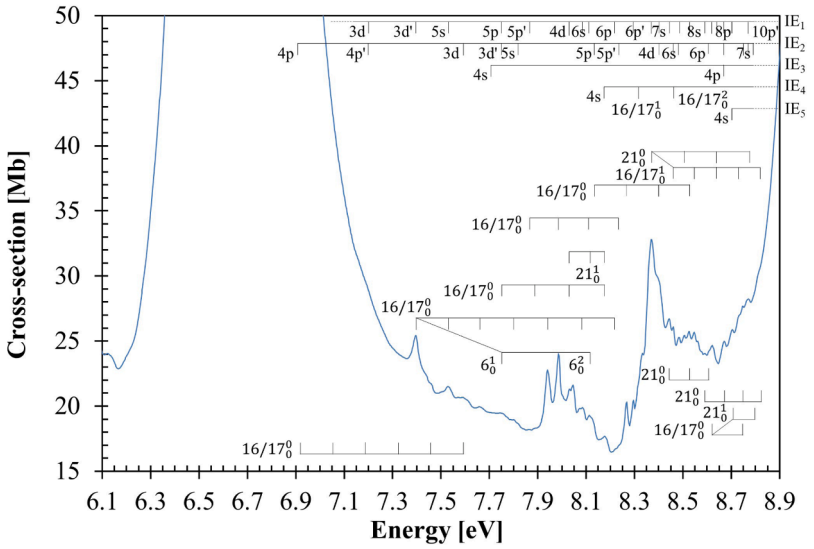

Fig. 4. Detail of the photoabsorption spectrum of 2-chlorotoluene in the 6.1–8.9 eV photon energy range with Rydberg series converging to $(6a'')^{-1}\ \widetilde{X}\ ^2A''$ (IE_1), $(5a'')^{-1}\widetilde{A}\ ^2A''$ (IE_2), $(27a')^{-1}\ \widetilde{B}\ ^2A'$ (IE_3), $(4a'')^{-1}\ \widetilde{C}\ ^2A''$ (IE_4) and $(26a')^{-1}\ \widetilde{D}\ ^2A'$ (IE_5). See text for details.

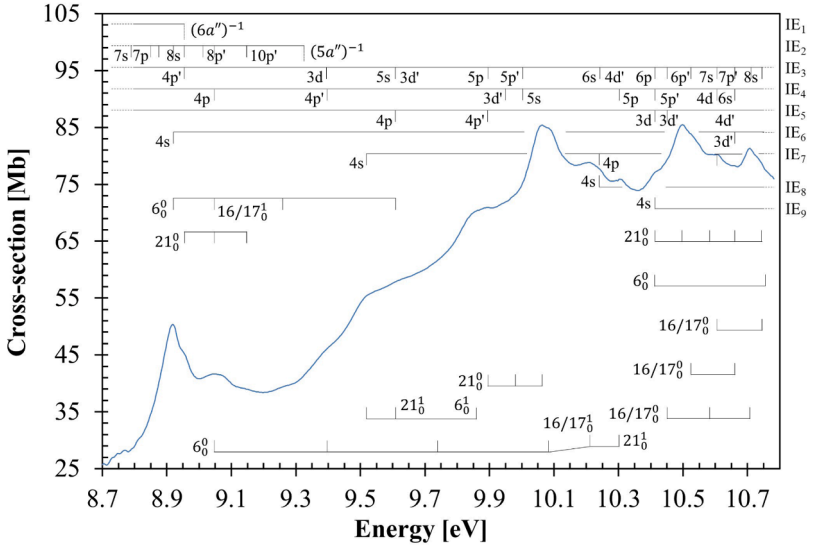

Fig. 5. Detail of the photoabsorption spectrum of 2-chlorotoluene in the 8.7–10.8 eV photon energy range with Rydberg series converging to $(6a'')^{-1}\ \widetilde{X}\ ^2A''$ (IE_1), $(5a'')^{-1}\widetilde{A}\ ^2A''$ (IE_2), $(27a')^{-1}\ \widetilde{B}\ ^2A'$ (IE_3), $(4a'')^{-1}\ \widetilde{C}\ ^2A''$ (IE_4), $(26a')^{-1}\ \widetilde{D}\ ^2A'$ (IE_5), $(25a')^{-1}\ \widetilde{E}\ ^2A'$ (IE_6), $(3a'')^{-1}\ \widetilde{F}\ ^2A''$ (IE_7), $(24a')^{-1}\ \widetilde{G}\ ^2A'$ (IE_8) and $(23a')^{-1}\ \widetilde{H}\ ^2A'$ (IE_9). See text for details.

bending $\nu''_{23}(a')$. Other vibrational modes have been assigned to C–Cl stretching/C–C in-plane bending, $\nu''_{18}(a')$, $\nu''_{19}(a')$ and $\nu''_{25}(a')$ with 0.132, 0.131 and 0.046 eV (1064, 1058 and 374 cm^{-1}) and C–CH_3/C–Cl in-plane bending, $\nu''_{26}(a')$ with 0.031 eV (248 cm^{-1}) (see Section 5.1).

The assignment of the different Rydberg orbitals based on their quantum defects and the associated features in the absorption spectrum, is obtained for the lowest experimental vertical ionisation energies (IEs) taken from the Penning ionisation data of Kishimoto and co-workers [11] to be 8.96 $(6a'')^{-1}$, 9.33 $(5a'')^{-1}$, 11.11 $(27a')^{-1}$, 11.52 $(4a'')^{-1}$, 12.04 $(26a')^{-1}$, 12.23 eV $(25a')^{-1}$, 12.70 eV $(3a'')^{-1}$, 13.54 eV $(24a')^{-1}$ and 13.81 eV $(23a')^{-1}$.

5. Results and discussion

The absolute photoabsorption spectrum of 2-chlorotoluene is shown in Fig. 1 in the energy range 4.0 to 10.8 eV, while expanded views of the spectrum are depicted in Figs. 2–5. The main absorption bands have been assigned to electronic excitations from the ground state to valence, mixed valence-Rydberg and Rydberg character molecular orbitals converging to the different ionic electronic states, $(6a'')^{-1}\ \widetilde{X}\ ^2A''$, $(5a'')^{-1}\widetilde{A}\ ^2A''$, $(27a')^{-1}\ \widetilde{B}\ ^2A'$, $(4a'')^{-1}\ \widetilde{C}\ ^2A''$, $(26a')^{-1}\ \widetilde{D}\ ^2A'$, $(25a')^{-1}\ \widetilde{E}\ ^2A'$, $(3a'')^{-1}\ \widetilde{F}\ ^2A''$, $(24a')^{-1}\ \widetilde{G}\ ^2A'$ and $(23a')^{-1}\ \widetilde{H}\ ^2A'$ (see Section 5.4). In the photon energy range 4.4–5.2 eV (Fig. 2) the spectrum shows extensive fine structure assigned to the C–C in plane bending, $\nu'_{23}(a')$ mode, while from 5.4 up to 10.8 eV (Fig. 3–5) the dominant modes are the C–H stretching (CH_3), $\nu'_6(a')$, C–H in-plane bending, $\nu'_{16}(a')/\nu'_{17}(a')$, and C–Cl stretching (C–CH_3 stretching and C–C in-plane bending), $\nu'_{21}(a')$. The photoabsorption features are dominated by the overlap of different Rydberg transitions, with the exception of the lowest-lying band (4.4–5.2 eV) which is valence in character. The TD-DFT calculation in Table 1 is compared with the experimental data, and a reasonably good level of agreement (to within ± 8 %) is noted. We have also checked the

Table 1
The most representative calculated vertical excitation energies (TD-DFT/B3LYP/aug-cc-pVDZ) and oscillator strengths of 2-chlorotoluene compared with the present experimental data. Energies in eV. See text for details.

2-chlorotoluene				E (eV) expt.[a]	Cross-section (Mb)
State	E (eV)	f_L	Dominant excitations		
$\widetilde{X}\ ^1A'$					
$2\ ^1A'$	5.083	0.004884	$1\pi^*(7a'') \leftarrow \pi/n_{Cl}(6a'')$ (38 %) + $2\pi^*(8a'') \leftarrow \pi/n_{Cl}(6a'')$ (25 %) + $2\pi^*(8a'') \leftarrow \pi/n_{Cl}(5a'')$ (20 %) + $1\pi^*(7a'') \leftarrow \pi/n_{Cl}(5a'')$ (17 %)	4.688	1.1
$3\ ^1A'$	5.660	0.047915	$2\pi^*(8a'') \leftarrow \pi/n_{Cl}(6a'')$ (36 %) + $1\pi^*(7a'') \leftarrow \pi/n_{Cl}(6a'')$ (35 %) + $1\pi^*(7a'') \leftarrow \pi/n_{Cl}(5a'')$ (20 %)	5.93(2)	25.34
$4\ ^1A'$	6.384	0.378069	$1\pi^*(7a'') \leftarrow \pi/n_{Cl}(5a'')$ (53 %) + $2\pi^*(8a'') \leftarrow \pi/n_{Cl}(6a'')$ (35 %)	6.64(4)	195.83
$5\ ^1A'$	6.479	0.569023	$2\pi^*(8a'') \leftarrow \pi/n_{Cl}(5a'')$ (65 %) + $1\pi^*(7a'') \leftarrow \pi/n_{Cl}(6a'')$ (23 %)	6.64(4)	195.83
$11\ ^1A'$	7.755	0.092630	$1\pi^*(7a'') \leftarrow \pi/n_{Cl}(4a'')$ (54 %) + $2\pi^*(8a'') \leftarrow \pi/n_{Cl}(4a'')$ (16 %) + $3\pi^*(10a'') \leftarrow \pi/n_{Cl}(6a'')$ (14 %)	7.398	25.38
$15\ ^1A'$	8.072	0.021186	$4p'(30a') \leftarrow \overline{n}_{Cl}/\sigma_{CC}$ (27a') (56 %) + $3\pi^*(10a'') \leftarrow \pi/n_{Cl}(5a'')$ (19 %) + $4p(29a') \leftarrow \overline{n}_{Cl}/\sigma_{CC}(27a')$ (12 %)	7.986	24.05
$19\ ^1A'$	8.718	0.029679	$7d/\pi^*(12a'') \leftarrow \pi/n_{Cl}(6a'')$ (63 %) + $1\pi^*(7a'') \leftarrow \pi(3a'')$ (24 %)	8.372	32.78
$27\ ^1A'$	9.079	0.046813	$4p(29a') \leftarrow \sigma_{CC/Cl}(25a')$ (68 %) + $4p/3d'(34a') \leftarrow \overline{n}_{Cl}/\sigma_{CC}(27a')$ (16 %)	8.920	50.39
$30\ ^1A'$	9.253	0.067569	$3p'(30a') \leftarrow \sigma_{CC/Cl}(26a')$ (82 %) + $3d'''/\pi^*(13a'') \leftarrow \pi/n_{Cl}(5a'')$ (12 %)	9.51(5)	55.17
$35\ ^1A'$	9.511	0.095353	$\sigma^*_{CCl}(31a') \leftarrow \sigma_{CC/Cl}(26a')$ (70 %)	9.90(0)	70.89
$44\ ^1A'$	9.984	0.053121	$3d(32a') \leftarrow \sigma_{CC/Cl}(25a')$ (89 %)		
$61\ ^1A'$	10.504	0.054361	$4s(28a') \leftarrow \sigma_{CC/CH}(23a')$ (57 %) + $3d(32a') \leftarrow \pi(3a'')$ (30 %)	10.064	85.40
$66\ ^1A'$	10.703	0.109594	$4p(29a') \leftarrow \sigma_{CC/CH}(23a')$ (87 %)	10.498	85.46

[a] the last decimal of the energy value is given in brackets for these less-resolved features;

level of accuracy by performing additional EOM-CCSD/aug-cc-pVDZ calculations (Table S2), with a selection of 2-chlorotoluene molecular orbitals in Fig. S4. No relevant differences are noted in the close comparison with TD-DFT/B3LYP/aug-cc-pVDZ level of theory results. The complete assignment of the fine structure associated with the electronic transitions are listed in Tables 2–5 and compared with previous work wherever possible.

The 2-chlorotolune photoabsorption bands in Fig. 1 are assigned to the $1\pi^*(7a'')/2\pi^*(8a'') \leftarrow \pi/n_{Cl}(6a'') +\ 2\pi^*(8a'')/1\pi^*(7a'') \leftarrow \pi/n_{Cl}(5a'')$, $(2\ ^1A' \leftarrow \widetilde{X}\ ^1A')$, $1\pi^*(8a'') \leftarrow \pi/n_{Cl}(6a'') +\ 1\pi^*(7a'') \leftarrow \pi/n_{Cl}(6a'') + 1\pi^*(7a'') \leftarrow \pi/n_{Cl}(5a'')$, $(3\ ^1A' \leftarrow \widetilde{X}\ ^1A')$, $2\pi^*(8a'') \leftarrow \pi/n_{Cl}(5a'') + 1\pi^*(7a'') \leftarrow \pi/n_{Cl}(6a'')$, $(5\ ^1A' \leftarrow \widetilde{X}\ ^1A')$, $1\pi^*(7a'')/2\pi^*(8a'') \leftarrow \pi/n_{Cl}(4a'') + 3\pi^*(10a'') \leftarrow \pi/n_{Cl}(6a'')$, $(11\ ^1A' \leftarrow \widetilde{X}\ ^1A')$, $4p'(30a')/4p(29a') \leftarrow \overline{n}_{Cl}(27a') + 3\pi^*(10a'') \leftarrow \pi/n_{Cl}(5a'')$, $(15\ ^1A' \leftarrow \widetilde{X}\ ^1A')$, $7d/\pi^*(12a'') \leftarrow \pi/n_{Cl}(6a'') +\ 1\pi^*(7a'') \leftarrow \pi(3a'')$, $(19\ ^1A' \leftarrow \widetilde{X}\ ^1A')$, $4p(29a') \leftarrow \sigma_{CC/Cl}(25a') +\ 4p/3d'(34a') \leftarrow \overline{n}_{Cl}/\sigma_{CC}(27a')$, $(27\ ^1A' \leftarrow \widetilde{X}\ ^1A')$, $3p'(30a') \leftarrow \sigma_{CC/Cl}(26a') + 3d'''/\pi^*(13a'') \leftarrow \pi/n_{Cl}(5a'')$, $(30\ ^1A' \leftarrow \widetilde{X}\ ^1A')$, $\sigma^*_{CCl}(31a') \leftarrow \sigma_{CC/Cl}(26a')$, $(35\ ^1A' \leftarrow \widetilde{X}\ ^1A')$, $4s(28a') \leftarrow \sigma_{CC/CH}(23a') + 3d(32a') \leftarrow \pi(3a'')$, $(61\ ^1A' \leftarrow \widetilde{X}\ ^1A')$ and, $4p(29a') \leftarrow \sigma_{CC/CH}(23a')$, $(66\ ^1A' \leftarrow \widetilde{X}\ ^1A')$ transitions (Table 1). The next sections include a detailed description of the different photoabsorption features, aided by our theoretical calculations.

5.1. The 4.5–7.0 eV photon energy range

The lowest-lying singlet-singlet valence transition, is assigned mainly to promotion of the chlorine lone pair orbital out-of-plane (n_{Cl}) with ring π(C=C) to the $1\pi^*/2\pi^*$ molecular orbitals, $1\pi^*(7a'')/2\pi^*(8a'') \leftarrow \pi/n_{Cl}(6a'') +\ 2\pi^*(8a'')/1\pi^*(7a'') \leftarrow \pi/n_{Cl}(5a'')$, $(2\ ^1A' \leftarrow \widetilde{X}\ ^1A')$, with a local cross-section of 1.1 Mb. The vertical excitation energy value of 4.688 eV is in reasonable agreement with the calculated value 5.083 eV as shown in Table 1. The oscillator strength value obtained at the EOM-CCSD level of theory (see Table S2) is lower than the TD-DFT calculation result, however with a rather close calculated energy to the experimental value.

Fig. 2 shows the fine structure due to vibronic excitation in the 4.4–5.2 eV energy region in greater detail than any previous measurements. The 0_0^0 origin of the band at 4.572 eV has been reported by Richard *et al.* [17] from resonant two-photon ionisation experiments, in excellent agreement with the present work. This band shows a large number of progressions (noted as p_n, $n = 1$–11) that are listed in Table 2 and have been assigned to the contribution of several 23_0^n ($n = 1$–7) progressions from the C–C in plane bending, $\nu'_{23}(a')$ mode, with an average spacing of 0.060 eV (484 cm^{-1}). Additional assignments from the torsion–vibrational coupling spectroscopic work of Richard *et al.* [17] are due to C–Cl stretching/C–C in-plane bending, $\nu'_{18}(a')$, $\nu'_{19}(a')$, $\nu'_{25}(a')$ and C–CH_3/C–Cl in-plane bending, $\nu'_{26}(a')$ modes. It is relevant to note that similar assignments from the unresolved internal rotational envelope of the methyl group have been reported for the three isomers of fluorotoluene [5–7], and so the differences reported in Table 1 may account for such contribution.

The geometry of 2-chlorotoluene in the first excited state together with bond lengths in Å and bond angles in (°), is depicted in Fig. S2. A close comparison with the molecular geometry of the ground state molecule (Fig. S1) shows no relevant methyl group rotation relative to the ring, which do not lead to hyperconjugation between the ring π^* MO and the methyl CH σ^* orbital in the LUMO. Such is supported by the calculated potential energy curves of both ground and first excited state (Fig. S8), showing similar minima position for every 120° rotation of the CH_3 group. However, the first excited state exhibits a lowering of ~ 420 cm^{-1} relative to the ground state internal barrier to rotation, in relatively good agreement with 337 cm^{-1} from Richard and co-workers [17].

Another interesting aspect relates to the close comparison between the neutral ground state and the first excited state lengthening of C2–C3, C3–C4, C4–C5 and C5–C6 bonds, from ~1.40 Å to ~1.43 Å (Figs. S1 and S2), and consequently a change in C2–C3–C4 and C4–C5–C6 angles, whereas C2 – Cl15 does not change appreciably (< 1 %). This is consistent with $\nu''_{23}(a')$ mode in the ground state, whereas no change is noted for the C1–C2–Cl15 angle (< 1 %) in the $(\widetilde{A}\ ^1A' \leftarrow \widetilde{X}\ ^1A')$ transition. This renders mainly C–C in-plane bending, $\nu'_{23}(a')$, while C–Cl stretching, $\nu'_{18}(a')/\nu'_{19}(a')/\nu'_{25}(a')$, and C–Cl bending modes, $\nu'_{26}(a')$, are not relevant upon electronic excitation from the ground state to the lowest-lying excited state of 2-chlorotoluene.

The second absorption band centred at 5.93(2) eV with a maximum cross-section of 25.34 Mb, is assigned to the valence excitation $1\pi^*(8a'') \leftarrow \pi/n_{Cl}(6a'') + 1\pi^*(7a'') \leftarrow \pi/n_{Cl}(6a'') + 1\pi^*(7a'') \leftarrow \pi/n_{Cl}(5a'')$, $(3\ ^1A' \leftarrow \widetilde{X}\ ^1A')$ with an oscillator strength of ≈ 0.0479 (Table 1), which is in good agreement with the EOM-CCSD/aug-cc-pVDZ calculation in Table S2, assigned to the $1\pi^*(8a'')/2\pi^*(9a'') \leftarrow \pi/n_{Cl}(6a'') + 1\pi^*(8a'') \leftarrow \pi/n_{Cl}(5a'')$, $(3\ ^1A' \leftarrow \widetilde{X}\ ^1A')$ transition with $f_L \approx 0.0445$. The 0_0^0 origin band is assigned at 5.69(3) eV (Table 3 and Fig. 3) and shows broad features

Table 2
Proposed vibrational assignments of 2-chlorotoluene absorption band in the photon energy range 4.4−5.2 eV[a]. Energies in eV. See text for details.

This work			Previous work [17] (assignment)
assignment	energy	ΔE (ν_{23})	
$1\pi^*(7a'')/2\pi^*(8a'')\leftarrow\pi/n_{Cl}(6a'') + 2\pi^*(8a'')/1\pi^*(7a'')\leftarrow\pi/n_{Cl}(5a'')$, $(2\ ^1A'\leftarrow\widetilde{X}\ ^1A')$			
$p_1 23_0^0$	4.52(9)(s)	0.0 (-0.043)	–
$p_2 23_0^0$	4.53(2)(s)	0.0 (-0.040)	–
$p_3 23_0^0$	4.53(4)(s)	0.0 (-0.038)	–
$p_4 23_0^0$	4.54(2)(w)	0.0 (-0.030)	–
$p_5 23_0^0$	4.545	0.0 (-0.027)	–
$p_6 23_0^0$	4.549	0.0 (-0.023)	–
$p_7 23_0^0$	4.552	0.0 (-0.020)	–
$p_8 23_0^0$	4.556	0.0 (-0.016)	–
$p_9 23_0^0$	4.562	0.0 (-0.010)	–
$p_{10} 23_0^0$	4.563	0.0 (-0.009)	–
$p_{11} 23_0^0$	4.57(0)(s)	0.0 (-0.002)	–
0_0^0	4.572	0.0	4.572 (0_0^0)
$p_1 23_0^1$	4.581	0.052	–
$p_2 23_0^1$	4.588	0.056	–
$p_3 23_0^1$	4.595	0.061	4.595 (38_0^2)
$p_4 23_0^1$ /26_0^1	4.60(1)(w)	0.059	4.603 (26_0^1)
$p_5 23_0^1$	4.60(7)(w)	0.062	4.606 (37_0^2)
$p_6 23_0^1$	4.60(9)(b,w)	0.060	–
$p_7 23_0^1$	4.61(2)(s)	0.060	–
$p_8 23_0^1$ /25_0^1	4.614	0.058	4.614 (25_0^1)
$p_9 23_0^1$	4.62(0)(s)	0.058	–
$p_{10} 23_0^1$	4.624	0.061	–
$p_{11} 23_0^1$	4.63(0)(s)	0.060	–
23_0^1	4.632	0.060	4.632 (23_0^1)
$p_1 23_0^2$	4.64(0)(s)	0.059	–
$p_2 23_0^2$	4.64(9)(s)	0.061	–
$p_3 23_0^2$	4.65(6)(s)	0.061	–
$p_4 23_0^2$	4.659	0.058	–
$p_5 23_0^2$	4.66(4)(s)	0.057	–
$p_6 23_0^2$	4.667	0.058	–
$p_7 23_0^2$	4.67(3)(s)	0.061	–
$p_8 23_0^2$	4.67(5)(s)	0.061	–
$p_9 23_0^2$	4.680	0.060	–
$p_{10} 23_0^2$	4.68(3)(s)	0.059	–
$p_{11} 23_0^2$ /19_0^1	4.688	0.058	4.689 (19_0^1)
23_0^2 /18_0^1	4.690	0.058	4.691 (18_0^1)
$p_1 23_0^3$	4.701	0.061	–
$p_2 23_0^3$	4.70(9)(w)	0.060	–
$p_3 23_0^3$	4.718	0.062	–
$p_4 23_0^3$	4.72(4)(s,w)	0.065	–
$p_5 23_0^3$	4.72(5)(s,w)	0.061	–
$p_6 23_0^3$	4.72(7)(w)	0.060	–
$p_7 23_0^3$	4.73(2)(s,w)	0.059	–
$p_8 23_0^3$	4.73(3)(w)	0.058	–
$p_9 23_0^3$	4.74(0)(b)	0.060	–
$p_{10} 23_0^3$	4.74(2)(b)	0.059	–
$p_{11} 23_0^3$	4.74(9)(w)	0.061	–
23_0^3	4.75(0)(w)	0.060	–
$p_1 23_0^4$	4.760	0.059	–
$p_2 23_0^4$	4.766	0.057	–
$p_3 23_0^4$	4.778	0.060	–
$p_4 23_0^4$	4.77(9)(w)	0.055	–
$p_5 23_0^4$	4.78(4)(w)	0.059	–
$p_6 23_0^4$	4.78(6)(b,w)	0.059	–
$p_7 23_0^4$	4.79(2)(s)	0.060	–
$p_8 23_0^4$	4.79(7)(s)	0.064	–
$p_9 23_0^4$	4.79(8)(b)	0.058	–
$p_{10} 23_0^4$	4.80(3)(s)	0.061	–
$p_{11} 23_0^4$	4.80(5)(w)	0.056	–
23_0^4	4.80(8)(w)	0.058	–
$p_1 23_0^5$	4.820	0.060	–
$p_2 23_0^5$	4.82(5)(w)	0.059	–
$p_3 23_0^5$	4.84(3)(w)	0.065	–
$p_4 23_0^5$	4.84(4)(w)	0.065	–
$p_5 23_0^5$	4.84(8)(s,w)	0.064	–
$p_6 23_0^5$	4.85(3)(s,b)	0.067	–
$p_7 23_0^5$	4.85(5)(s,b)	0.063	–
$p_8 23_0^5$	4.85(6)(s,b)	0.059	–
$p_9 23_0^5$	4.86(2)(s,w)	0.064	–
$p_{10} 23_0^5$	4.86(8)(w)	0.065	–
$p_1 23_0^6$	4.87(7)(s)	0.057	–
$p_2 23_0^6$	4.88(8)(b,w)	0.063	–
$p_3 23_0^6$	4.90(1)(s,w)	0.058	–
$p_4 23_0^6$	4.90(7)(s,w)	0.063	–
$p_5 23_0^6$	4.91(2)(b,w)	0.064	–
$p_6 23_0^6$	4.91(4)(b,w)	0.061	–
$p_7 23_0^6$	4.91(5)(s)	0.060	–
$p_8 23_0^6$	4.92(2)(w)	0.066	–
$p_9 23_0^6$	4.92(8)(w)	0.066	–
$p_1 23_0^7$	4.93(6)(s,w)	0.059	–
$p_2 23_0^7$	4.94(2)(s,w)	0.054	–
$p_3 23_0^7$	4.96(5)(s,w)	0.064	–
$p_4 23_0^7$	4.97(0)(s,w)	0.063	–
$p_5 23_0^7$	4.97(3)(s,w)	0.061	–
$p_6 23_0^7$	4.97(7)(s,w)	0.063	–
$p_7 23_0^7$	4.98(0)(s,w)	0.065	–
	$\overline{\Delta E}$	0.060	

[a] (s) shoulder structure; (w) weak feature; (b) broad feature (the last decimal of the energy value is given in brackets for these less-resolved features);

assigned to the main vibrational modes C–H stretching (CH_3), $\nu'_6(a')$, C–H in-plane bending, $\nu'_{16}(a')/\nu'_{17}(a')$, and C–Cl stretching (C–CH_3 stretching and C–C in-plane bending), $\nu'_{21}(a')$ (Table 3). The band also contains features assigned to the lowest-lying Rydberg members (4s) and their associated fine structure converging to $(6a'')^{-1}\ \widetilde{X}\ ^2A''$ and $(5a'')^{-1}\widetilde{A}\ ^2A''$ states (see Section 5.4). Additional assignments within the second absorption band include some quanta of the C=C, $\nu'_7(a')$, and C–C, $\nu'_1(a')$, stretching modes.

The relatively broad nature of the features may be indicative of a more valence character, however, the one order of magnitude lower oscillator strength (Table 1) relative to the next valence contribution, $(5\ ^1A'\leftarrow\widetilde{X}\ ^1A')$, may also render a Rydberg character (Section 5.4), the latter predicted by the calculations as $(6\ ^1A''\leftarrow\widetilde{X}\ ^1A')$ at ~6.403 eV with an oscillator strength $f_L \approx 0.0011$ (see Table S1).

The most intense absorption band with a maximum at 6.64(4) eV and a cross-section of 195.83 Mb (Fig. 1) is assigned to a valence $2\pi^*(8a'')\leftarrow\pi/n_{Cl}(5a'') + 1\pi^*(7a'')\leftarrow\pi/n_{Cl}(6a'')$, $(5\ ^1A'\leftarrow\widetilde{X}\ ^1A')$ transition with an oscillator strength $f_L \approx 0.5690$; the calculations also predict a valence transition with the same character, $1\pi^*(7a'')\leftarrow\pi/n_{Cl}(5a'') + 2\pi^*(8a'')\leftarrow\pi/n_{Cl}(6a'')$, $(5\ ^1A'\leftarrow\widetilde{X}\ ^1A')$, with an oscillator strength value of $f_L \approx 0.3781$, although at a slightly lower energy (6.384 eV) than the former (6.479 eV). These transitions are indicated in Table 1.

We also note from the EOM-CCSD/aug-cc-pVDZ calculation in Table S2 that a Rydberg character is not expected to contribute to the spectrum. However, the quantum defects obtained for the features in this absorption band suggest the presence of Rydberg series converging to the different ionisation energies (see Section 5.4). This is in agreement with the TD-DFT result in Table S1 for the $(7\ ^1A''\leftarrow\widetilde{X}\ ^1A')$ transition at ~6.587 eV and $f_L \approx 0.0124$. The 0_0^0 origin band is assigned at 6.50(5) eV and shows two quanta of C–H in-plane bending, $\nu'_{16}(a')/\nu'_{17}(a')$ modes (Fig. 3 and Table 3).

5.2. The 7.0–9.4 eV photon energy range

This energy range comprises four electronic transitions centred at 7.398, 7.986, 8.372 and 8.920 eV (Figs. 1, 4 and 5), which are assigned to valence and mixed valence-Rydberg transitions with cross-section values of 25.38, 24.05, 32.78 and 50.39 Mb, respectively (Table 1). The calculations show that the lowest electronic state is manly valence, although it may contain 14 % of Rydberg-like character. However, some of the features have been assigned to Rydberg series converging to the ionic electronic ground and ionic electronic first excited states (Table 4). The 0_0^0 origins of these bands are at 7.395, 7.86(2), 8.13(3) and 8.920 eV, and are accompanied by excitation of C–H stretching (CH_3), $\nu'_6(a')$ and C–H in-plane bending, $\nu'_{16}(a')/\nu'_{17}(a')$ modes, with mean energy values of 0.360 and 0.136 eV (Tables 4 and 5).

5.3. The 8.7–10.8 eV photon energy range

The absorption features in this photon energy region are classified as valence and Rydberg (Section 5.4) with extensive vibrational fine structure. An expanded plot of the current measured photoabsorption spectrum is presented in Fig. 5, with our proposed assignments summarised in Tables 4 and 5. In this energy region, the features appear too broad for the major Rydberg character, which are expected to be narrower. This is due to their energy positions being superimposed either on the vibrational progressions of other Rydberg series contributing to the spectrum or on valence states. The only assigned valence excited state, $\sigma^*_{CCl}(31a')\leftarrow\sigma_{CC/Cl}(26a')$, $(35\ ^1A'\leftarrow\widetilde{X}\ ^1A')$, has a 0_0^0 transition at 9.9(0) eV, with a cross-section of 70.89 Mb. From the calculations in Table 1, the other transitions have been assigned to Rydberg $3p'(30a')\leftarrow\sigma_{CC/Cl}(26a')+3d'''/\pi^*(13a'')\leftarrow\pi/n_{Cl}(5a'')$, $(30\ ^1A'\leftarrow\widetilde{X}\ ^1A')$, $4s(28a')\leftarrow\sigma_{CC/CH}(23a')+3d(32a')\leftarrow\pi(3a'')$, $(61\ ^1A'\leftarrow\widetilde{X}\ ^1A')$ and $4p(29a')\leftarrow\sigma_{CC/CH}(23a')$, $(66\ ^1A'\leftarrow\widetilde{X}\ ^1A')$, with oscillator strengths of ≈ 0.0676, ≈ 0.05436 and ≈ 0.1096, respectively, and they show relevant fine structure superimposed on a diffuse background. The absorption bands appear to be superimposed on an underlying absorption continuum that may be attributed to the dissociative character of the $\sigma^*_{CCl}(31a')\leftarrow\sigma_{CC/Cl}(26a')$ transition, as well as the photoionisation contribution of the $(6a'')^{-1}$ $\widetilde{X}\ ^2A''$ and $(5a'')^{-1}\widetilde{A}\ ^2A''$ ionic states. The transitions are accompanied by fine structure, which will be discussed below in Section 5.4 for the main modes being active in those electronic states.

5.4. Rydberg transitions

The Rydberg transitions converging to the different ionic states of 2-chlorotoluene have been tentatively assigned in Table 6 according to the position of the features and the quantum defects obtained from the Rydberg formula, i.e., $E_n = IE - \frac{R}{(n-\delta)^2}$, where IE is the ionisation energy of a given MO, n is the principal quantum number of the Rydberg orbital of energy E_n, R is the Rydberg constant (13.61 eV), and δ is the quantum defect resulting from the penetration of the Rydberg orbital into the core.

The Rydberg character of the absorption features in the spectrum is prominently observed above 5.6 eV, with their intensities decreasing as n increases. The fine structure noted in the photon energy region of the Rydberg series (Fig. 3–5), shows upon a close inspection that most of the vibronic transitions appear particularly enhanced. No previous works have provided Rydberg assignments for 2-chlorotoluene, and so the fine structure discernible on the different Rydberg transitions up to 10.8 eV, which are listed in Tables 3–5, are the most complete analysis to date. In Tables 4 and 5, we note that the assignment of some of the electronic transitions provided by the calculations are not in agreement with the suggested Rydberg states obtained from the quantum defects estimate. As an example, we note in Table 4 that the calculated $(15\ ^1A'\leftarrow\widetilde{X}\ ^1A')$ transition yielding $4p'(30a')/4p(29a')$, does not match the experimental feature at 7.86(2) eV which rather has been assigned to $5p'(6a'')^{-1}$ (Fig. 4).

The lowest-lying Rydberg transition ($n = 3$) converging to the ionic electronic ground state IE_1, $(6a'')^{-1}$, is assigned to the $(4s\leftarrow6a'')$ excitation, with the first member at 5.703 eV and having a quantum defect $\delta = 1.96$. Other higher-order Rydberg members of the ns series, up to $n = 8$, are also reported in Table 6.

The first members of the two np $(np\leftarrow6a'')$ and $(np'\leftarrow6a'')$ series have

Table 3
Proposed vibrational assignments of 2-chlorotoluene absorption band in the photon energy range 5.4−6.8 eV[a]. Energies in eV. See text for details.

assignment	energy	ΔE (ν_1')	ΔE (ν_6')	ΔE (ν_7')	ΔE ($\nu_{16/17}'$)	ΔE (ν_{21}')
$1\pi^*(7a'')\leftarrow\pi/n_{Cl}(5a'')+2\pi^*(8a'')\leftarrow\pi/n_{Cl}(6a'')$, $(4\ ^1A'\leftarrow\widetilde{X}\ ^1A')$						
0_0^0	5.69(3)(s)	–	–	–	–	–
$4s(6a'')^{-1}$	5.703	–	–	–	–	–
$16\ /17_0^1$	5.83(5)(s)	–	–	–	0.142	–
$4s(6a'')^{-1}16\ /17_0^1$	5.85(4)(s,b)	–	–	–	0.151	–
$16\ /17_0^121_0^1$	5.93(2)(b)	–	–	–	–	0.097
6_0^1	6.072	–	0.379	–	–	–
$16\ /17_0^121_0^17_0^1$	6.13(3)(b)	–	–	0.201	–	–
$16\ /17_0^11_0^1$	6.21(6)(s)	0.381	–	–	–	–
$16\ /17_0^121_0^17_0^2$	6.33(1)(s,w)	–	–	0.198	–	–
						–
$4s(5a'')^{-1}$	5.93(2)(b)	–	–	–	–	–
$16\ /17_0^1$	6.072	–	–	–	0.140	–
$16\ /17_0^2$	6.21(6)(s)	–	–	–	0.144	–
$2\pi^*(8a'')\leftarrow\pi(5a'')+1\pi^*(7a'')\leftarrow\pi/n_{Cl}(6a'')$, $(5\ ^1A'\leftarrow\widetilde{X}\ ^1A')$						
$0_0^0\ /4p(6a'')^{-1}$	6.50(5)(s)	–	–	–	–	–
$16\ /17_0^1$	6.64(4)(b)	–	–	–	0.139	–
$16\ /17_0^2$	6.77(9)(b)	–	–	–	0.135	–
$/4p'(6a'')^{-1}$						
	$\overline{\Delta E}$	0.381	0.379	0.200	0.142	0.097

[a] (s) shoulder structure; (b) broad structure; (w) weak feature (the last decimal of the energy value is given in brackets for these less-resolved features);

Table 4
Proposed vibrational assignments of 2-chlorotoluene valence and mixed valence-Rydberg series converging to the different ionic states in the photon energy range 6.1−8.9 eV[a]. Energies in eV. See text for details.

assignment	energy	ΔE (ν_6')	ΔE ($\nu_{16/17}'$)	ΔE (ν_{21}')
$4p(5a'')^{-1}$	6.90(7)(s,w)	–	–	–
$16/17_0^1$	7.05(3)(s,w)	–	0.146	–
$16/17_0^2$	7.18(3)(s)	–	0.130	–
$16/17_0^3$	7.32(3)(s)	–	0.140	–
$16/17_0^4$	7.45(3)(s)	–	0.130	–
$16/17_0^5$	7.59(5)(s)	–	0.142	–
$1\pi^*(7a'')/2\pi^*(8a'')\leftarrow\pi/n_{Cl}(4a'') + 3\pi^*(10a'')\leftarrow\pi/n_{Cl}(6a''), (11\ ^1A'\leftarrow\widetilde{X}\ ^1A')$				
$0_0^0/3d'(6a'')^{-1}$	7.395	–	–	–
$16/17_0^1/5s(6a'')^{-1}$	7.53(0)(b)	–	0.135	–
$16/17_0^2$	7.66(5)(b)	–	0.135	–
$6_0^1/5p(6a'')^{-1}/3d'(5a'')^{-1}$	7.74(4)(b)	0.349	–	–
$16/17_0^3$	7.80(5)(s)	–	0.140	–
$16/17_0^4$	7.940	–	0.135	–
$16/17_0^5/4d'(6a'')^{-1}$	8.08(5)(w)	–	0.145	–
$6_0^2/6s(6a'')^{-1}$	8.11(4)(w)	0.370	–	–
$16/17_0^6/6p(6a'')^{-1}$	8.22(2)(s,w)	–	0.137	–
$5p(6a'')^{-1}/3d'(5a'')^{-1}$	7.74(4)(b)	–	–	–
$16/17_0^1$	7.89(2)(w)	–	0.148	–
$16/17_0^2/4d(6a'')^{-1}$	8.030	–	0.138	–
$16/17_0^3/4d(6a'')^{-1}16/17_0^1$	8.178	–	0.148	–
$4p'(30a')/4p(29a')\leftarrow\overline{n}_{Cl}/\sigma_{CC}(27a') + 3\pi^*(10a'')\leftarrow\pi/n_{Cl}(5a''), (15\ ^1A'\leftarrow\widetilde{X}\ ^1A')$				
$0_0^0/5p'(6a'')^{-1}$	7.86(2)(s,w)	–	–	–
$16/17_0^1$	7.986	–	0.124	–
$16/17_0^2/6s(6a'')^{-1}$	8.11(4)(w)	–	0.128	–
$16/17_0^3/5p'(5a'')^{-1}/6s(6a'')^{-1}16/17_0^1$	8.23(5)(s,w)	–	0.121	–
$4d(6a'')^{-1}$	8.030	–	–	–
21_0^1	8.11(4)(w)	–	–	0.084
$16/17_0^1$	8.178	–	0.148	–
$7d/\pi^*(12a'')\leftarrow\pi/n_{Cl}(6a'') + 1\pi^*(7a'')\leftarrow\pi(3a''), (19\ ^1A'\leftarrow\widetilde{X}\ ^1A')$				
$0_0^0/5p(5a'')^{-1}$	8.13(3)(s,w)	–	–	–
$16/17_0^1$	8.268	–	0.135	–
$5d'(6a'')^{-1}/4d(5a'')^{-1}/16/17_0^2$	8.39(7)(s)	–	0.129	–
$7p'(6a'')^{-1}/16/17_0^3/5d'(6a'')^{-1}/4d(5a'')^{-1}16/17_0^1$	8.527	–	0.130	–
$4s(4a'')^{-1}$	8.178	–	–	–
$16/17_0^1$	8.31(6)(s)	–	0.138	–
$4d'(5a'')^{-1}/16/17_0^2$	8.460	–	0.144	–
$5d(6a'')^{-1}$	8.372	–	–	–
$21_0^1/4d'(5a'')^{-1}/16/17_0^2$	8.460	–	–	0.088
$16/17_0^1$	8.507	–	0.135	–
$21_0^2/4d'(5a'')^{-1}/16/17_0^221_0^1$	8.548	–	–	0.088
$21_0^3/16/17_0^2/4d'(5a'')^{-1}/16/17_0^221_0^2$	8.63(7)(s,w)	–	0.130	0.089
$21_0^4/16/17_0^2/4d'(5a'')^{-1}/16/17_0^221_0^2$	8.73(4)(s)	–	–	0.097
$21_0^5/16/17_0^2/4d'(5a'')^{-1}/16/17_0^221_0^2$	8.82(1)(s)	–	–	0.087
$7s(6a'')^{-1}$	8.443	–	–	–
$21_0^1/7p'(6a'')^{-1}$	8.527	–	–	0.084
$21_0^2/6p(5a'')^{-1}/7p'(6a'')^{-1}21_0^1$	8.60(7)(s)	–	–	0.080
$8s(6a'')^{-1}$	8.58(9)(w)	–	–	–
$21_0^1/7d(6a'')^{-1}/6p'(5a'')^{-1}/4p(27a')^{-1}$	8.670	–	–	0.081
$21_0^2/7d(6a'')^{-1}21_0^1/6p'(5a'')^{-1}21_0^1/4p(27a')^{-1}21_0^1$	8.750	–	–	0.080
$21_0^3/7d(6a'')^{-1}21_0^2/6p'(5a'')^{-1}21_0^2/4p(27a')^{-1}21_0^2$	8.82(5)(s)	–	–	0.075
$8p(6a'')^{-1}$	8.622	–	–	–
$21_0^1/9p(6a'')^{-1}/4s(26a')^{-1}$	8.707	–	–	0.085
$16/17_0^1/5d(5a'')^{-1}$	8.750	–	0.128	–
$21_0^2/7s(5a'')^{-1}/9p(6a'')^{-1}21_0^1/4s(26a')^{-1}21_0^1$	8.79(6)(s)	–	–	0.089
	$\overline{\Delta E}$	0.360	0.136	0.085

[a] (s) shoulder structure; (w) weak feature; (b) broad structure (the last decimal of the energy value is given in brackets for these less-resolved features);

absorption features at 6.50(5) eV and 6.77(9) eV (δ = 1.65 and 1.50). Table 6 also includes two nd ($nd\leftarrow6a''$) and ($nd'\leftarrow6a''$) series (n = 3–7), where the $n = 3$ features have been assigned at 7.20(0) and 7.395 eV (δ = 0.22 and 0.05). Other transitions to the *nd* and *nd'* Rydberg members, up to $n = 7$ and 6, are also discernible. The features at 7.74(4), 8.707, 8.771, 8.670 and 8.39(7) eV can also be assigned to $3d'(5a'')^{-1}$, $4s(26a')^{-1}$, $5d'(5a'')^{-1}$, $6p'(5a'')^{-1}/4p(27a')^{-1}$ and $4d(5a'')^{-1}$.

The Rydberg series converging to the ionic electronic first excited state IE_2, $(5a'')^{-1}$, are listed in Table 6, and have been assigned to the (ns, $np, np', nd, nd'\leftarrow5a''$) transitions. The first members of these series (either $n = 4$ or $n = 3$) are associated with features at 5.93(2) eV ($\delta = 2.00$), 6.90 (7) eV ($\delta = 1.63$), 7.19(2) eV ($\delta = 1.48$), 7.59(5) eV ($\delta = 0.20$) and 7.74

Table 5
Proposed vibrational assignments of 2-chlorotoluene valence and Rydberg series converging to the different ionic states in the photon energy range 8.8−10.8 eV[a]. Energies in eV. See text for details.

assignment	energy	ΔE (ν_6')	ΔE ($\nu_{16/17}'$)	ΔE (ν_{21}')
$4p(29a')\leftarrow\sigma_{CC/Cl}(25a') + 4p/3d'(34a')\leftarrow\bar{n}_{Cl}/\sigma_{CC}(27a'), (27\ ^1A'\leftarrow\tilde{X}\ ^1A')$				
$4s(25a')^{-1}/6d(5a'')^{-1}$	8.920	–	–	–
$16/17_0^1$	9.04(7)(b)	–	0.127	–
6_0^1	9.26(3)(b,w)	0.343	–	–
$6_0^2/5s(27a')^{-1}/3d'(27a')^{-1}/4p(26a')^{-1}$	9.61(5)(b)	0.352	–	–
$8s(5a'')^{-1}/6d'(5a'')^{-1}/4p'(27a')^{-1}$	8.95(5)(s)	–	–	–
$21_0^1/7d'(5a'')^{-1}/4p(4a'')^{-1}$	9.04(7)(b)	–	–	0.092
$21_0^2/7d'(5a'')^{-1}21_0^1/10p'(5a'')^{-1}$	9.14(7)(b,w)	–	0.130	0.100
$4p(4a'')^{-1}$	9.04(7)(b)	–	–	–
$6_0^1/4p'(4a'')^{-1}$	9.39(6)(s,w)	0.349	–	–
$6_0^2/4p'(4a'')^{-1}6_0^1$	9.74(3)(s,w)	0.347	–	–
$6_0^3/4p'(4a'')^{-1}6_0^2$	10.08(8)(s)	0.345	–	–
$6_0^316/17_0^1/4p'(4a'')^{-1}6_0^216/17_0^1$	10.21(3)(w)	–	0.125	–
$6_0^316/17_0^121_0^1/4p'(4a'')^{-1}6_0^216/17_0^1/21_0^1$	10.30(2)(s)	–	–	0.089
$3p'(30a')\leftarrow\sigma_{CC/Cl}(26a') + 3d'''/\pi^*(13a'')\leftarrow\pi/n_{Cl}(5a''), (30\ ^1A'\leftarrow\tilde{X}\ ^1A')$				
$4s(3a'')^{-1}$	9.51(5)(s)	–	–	–
$21_0^1/5s(27a')^{-1}/3d'(27a')^{-1}/4p(26a')^{-1}$	9.61(5)(b)	–	–	0.100
6_0^1	9.86(0)(b,w)	0.345	–	–
$\sigma^*_{CCl}(31a')\leftarrow\sigma_{CC/Cl}(26a'), (35\ ^1A'\leftarrow\tilde{X}\ ^1A')$				
$4s(28a')\leftarrow\sigma_{CC/CH}(23a') + 3d(32a')\leftarrow\pi(3a''), (61\ ^1A'\leftarrow\tilde{X}\ ^1A')$				
$0_0^0/5p(27a')^{-1}/4p'(26a')^{-1}$	9.90(0)(s)	–	–	–
21_0^1	9.98(3)(s)	–	–	0.083
21_0^2	10.064	–	–	0.081
$6p'(27a')^{-1}/3d'(26a')^{-1}$	10.45(4)(s,w)	–	–	–
$21_0^24s(23a')^{-1}/16/17_0^1$	10.58(3)(b,w)	–	0.129	–
$16/17_0^1/6d(27a')^{-1}$	10.707	–	0.124	–
$5d(27a')^{-1}$	10.52(5)(s)	–	–	–
$16/17_0^1/7p'(27a')^{-1}/6s(4a'')^{-1}/4d'(4a'')^{-1}/3d'(25a')^{-1}$	10.66(5)(w)	–	0.140	–
$7s(27a')^{-1}/4d(4a'')^{-1}/4p'(3a'')^{-1}$	10.60(6)(s)	–	–	–
$16/17_0^1/8s(27a')^{-1}$	10.73(9)(s)	–	0.133	–
$4p(29a')\leftarrow\sigma_{CC/CH}(23a'), (66\ ^1A'\leftarrow\tilde{X}\ ^1A')$				
$4s(23a')^{-1}$	10.41(5)(s)	–	–	–
21_0^1	10.498	–	–	0.083
21_0^2	10.58(3)(b,w)	–	–	0.085
$21_0^3/7p'(27a')^{-1}/6s(4a'')^{-1}/4d'(4a'')^{-1}/3d'(25a')^{-1}$	10.66(5)(w)	–	–	0.082
$21_0^4/8s(27a')^{-1}$	10.73(9)(s)	–	–	0.074
6_0^1	10.75(8)(s)	0.343	–	–
	$\overline{\Delta E}$	0.346	0.130	0.087

[a] (b) broad structure; (w) weak feature; (s) shoulder structure (the last decimal of the energy value is given in brackets for these less-resolved features);

(4) eV ($\delta = 0.04$) (Table 6). We note that features at 8.95(5) and 8.920 eV can also be assigned to 6d'$(5a'')^{-1}$/4p'$(27a')^{-1}$ and 4s$(25a')^{-1}$.

The Rydberg series converging to the ionic electronic second excited state IE_3, $(25a')^{-1}$, have been assigned to the $(ns, np, np', nd, nd' \leftarrow 27a')$ transitions. The first members of these series (either $n = 4$ or $n = 3$) have features at 7.71(3) eV ($\delta = 2.00$), 8.670 eV ($\delta = 1.64$), 8.95(5) eV ($\delta = 1.49$), 9.39(6) eV ($\delta = 0.18$) and 9.61(5) eV (δ = -0.02) (Table 6). The features at 9.39(6), 9.61(5), 9.90(0), 10.00(7), 10.23(4), 10.41(5), 10.45(4), 10.60(6) and 10.66(5) eV can also assigned to the Rydberg 4p'$(4a'')^{-1}$, 3d'$(27a')^{-1}$/4p$(26a')^{-1}$, 4p'$(26a')^{-1}$, 5s$(4a'')^{-1}$, 4d'$(27a')^{-1}$/4p$(3a'')^{-1}$/4s$(24a')^{-1}$, 5p'$(4a'')^{-1}$/3d$(26a')^{-1}$/4s$(23a')^{-1}$, 3d'$(26a')^{-1}$, 4d$(4a'')^{-1}$ and 6s$(4a'')^{-1}$/4d'$(4a'')^{-1}$/3d'$(25a')^{-1}$.

The Rydberg series converging to IE_4, $(4a'')^{-1}$, IE_5, $(26a')^{-1}$, and IE_6, $(26a')^{-1}$, have been assigned to the $(ns, np, np', nd, nd' \leftarrow 4a'')$, $(ns, np, np', nd, nd' \leftarrow 26a')$ and $(ns, nd' \leftarrow 25a')$ transitions. These Rydberg series show only a few members up to $n = 6$ (Table 6).

Finally, Table 6 lists the Rydberg series converging to IE_7, $(3a'')^{-1}$, IE_8, $(24a')^{-1}$, and IE_9, $(23a')^{-1}$, and have been assigned to the $(ns, np, np' \leftarrow 3a'')$, $(ns \leftarrow 24a')$ and $(ns \leftarrow 23a')$ transitions.

The absorption spectrum containing the Rydberg excitations is rich in fine structure from the different vibronic transitions, with detailed assignments in Tables 3–5. The most representative contributions are from the C–H stretching (CH_3), $\nu_6'(a')$, C–H in-plane bending, $\nu_{16}'(a')/\nu_{17}'(a')$, and C–Cl stretching (C–CH_3 stretching and C–C in-plane bending), $\nu_{21}'(a')$ modes. The assignments of vibrational features associated with most of the transitions that involve progressions in ν_{16}' and ν_{17}' have been labelled $16/17_0^1$, due to similar values (almost degenerate) of their activation energies in the neutral electronic ground state [13,14] (see also Table S3). In Tables 3/4/5, the vibronic assignments of the Rydberg series converging to the different ionic states show progressions and combination bands involving ν_6', $\nu_{16/17}'$ and ν_{21}', with average frequencies of 3057/2904/2791 cm^{-1} (0.379/0.360/0.346 eV), 1145/1097/1049 cm^{-1} (0.142/0.136/0.130 eV) and 782/686/702 cm^{-1} (0.097/0.085/0.087 eV), respectively, relative to their values in the neutral ground state, 3032.8 cm^{-1} (0.376 eV), 1173.5/1147.4 cm^{-1} (0.146/0.142 eV) and 810.5 cm^{-1} (0.101 eV).

5.5. Potential energy curves along the C=C, C–H and C–Cl coordinates

The potential energy curves (PECs) for the nine lowest-lying singlet excited states of 2-chlorotoluene, plotted following the vibrational modes C=C stretching, $\nu_7'(a')$, C–H in-plane bending, $\nu_{17}'(a')$, and C–Cl

Table 6

Energy values (eV), quantum defects (δ) and assignments of the Rydberg series converging to $(6a'')^{-1}\ \widetilde{X}\ ^2A''$, $(5a'')^{-1}\widetilde{A}\ ^2A''$, $(27a')^{-1}\ \widetilde{B}\ ^2A'$, $(4a'')^{-1}\ \widetilde{C}\ ^2A''$, $(26a')^{-1}\ \widetilde{D}\ ^2A'$, $(25a')^{-1}\ \widetilde{E}\ ^2A'$, $(3a'')^{-1}\ \widetilde{F}\ ^2A''$, $(24a')^{-1}\ \widetilde{G}\ ^2A'$ and $(23a')^{-1}\ \widetilde{H}\ ^2A'$ of 2-chlorotoluene. See text for details.

E_n	δ	assignment	E_n	δ	assignment	E_n	δ	assignment
$IE_1 = 8.96$ eV $(6a'')^{-1}$			$IE_2 = 9.33$ eV $(5a'')^{-1}$			$IE_3 = 11.11$ eV $(27a')^{-1}$		
$(ns \leftarrow 6a'')$			$(ns \leftarrow 5a'')$			$(ns \leftarrow 27a')$		
5.703	1.96	4s	5.93(2)(b)	2.00	4s	7.71(3)(w)	2.00	4s
7.53(0)(b)	1.92	5s	7.82(0)(s)	2.00	5s	9.61(5)(b)	1.98	5s
8.11(4)(w)	1.99	6s	8.483	1.99	6s	10.23(4)(s,b)	2.06	6s
8.443	1.87	7s	8.79(6)(s)	1.95	7s	10.60(6)(s)	1.81	7s
8.58(9)(w)	1.94	8s	8.95(5)(s)	1.98	8s	10.73(9)(s)	1.94	8s
$(np \leftarrow 6a'')$			$(np \leftarrow 5a'')$			$(np \leftarrow 27a')$		
6.50(5)(s)	1.65	4p	6.90(7)(s,w)	1.63	4p	8.670	1.64	4p
7.74(4)(b)	1.65	5p	8.13(3)(s,w)	1.63	5p	9.90(0)(s)	1.65	5p
8.22(2)(s,w)	1.71	6p	8.60(7)(s)	1.66	6p	10.41(5)(s)	1.58	6p
8.483	1.66	7p	8.85(6)(s,w)	1.64	7p	–	–	–
8.622	1.65	8p	–	–	–	–	–	–
8.707	1.67	9p	–	–	–	–	–	–
$(np' \leftarrow 6a'')$			$(np' \leftarrow 5a'')$			$(np' \leftarrow 27a')$		
6.77(9)(s)	1.50	4p'	7.19(2)(s)	1.48	4p'	8.95(5)(s)	1.49	4p'
7.86(2)(s,w)	1.48	5p'	8.23(5)(s,w)	1.47	5p'	10.00(7)(s,w)	1.49	5p'
8.296	1.47	6p'	8.670	1.46	6p'	10.45(4)(s,w)	1.45	6p'
8.527	1.39	7p'	8.87(8)(s)	1.51	7p'	10.66(5)(w)	1.48	7p'
8.63(7)(s,w)	1.51	8p'	9.01(7)(s,w)	1.41	8p'	–	–	–
–	–	9p'	–	–	–	–	–	–
8.771	1.51	10p'	9.14(7)(b,w)	1.38	10p'	–	–	–
$(nd \leftarrow 6a'')$			$(nd \leftarrow 5a'')$			$(nd \leftarrow 27a')$		
7.20(0)(s,w)	0.22	3d	7.59(5)(w)	0.20	3d	9.39(6)(s,w)	0.18	3d
8.030	0.17	4d	8.39(7)(s)	0.18	4d	–	–	–
8.372	0.19	5d	8.750	0.16	5d	10.52(5)(s)	0.18	5d
8.56(0)(s)	0.17	6d	8.920	0.24	6d	10.707	0.20	6d
8.670	0.15	7d	–	–	–	–	–	–
$(nd' \leftarrow 6a'')$			$(nd' \leftarrow 5a'')$			$(nd' \leftarrow 27a')$		
7.395	0.05	3d'	7.74(4)(b)	0.04	3d'	9.61(5)(b)	-0.02	3d'
8.08(5)(w)	0.06	4d'	8.460	0.05	4d'	10.23(4)(s,b)	0.06	4d'
8.39(7)(s)	0.08	5d'	8.771	0.07	5d'	–	–	–
8.58(0)(s,w)	0.02	6d'	8.95(5)(s)	-0.02	6d'	–	–	–
–	–	–	9.04(7)(b)	0.07	7d'	–	–	–
$IE_4 = 11.52$ eV $(4a'')^{-1}$			**$IE_5 = 12.04$ eV** $(26a')^{-1}$			**$IE_6 = 12.23$ eV** $(25a')^{-1}$		
$(ns \leftarrow 4a'')$			$(ns \leftarrow 26a')$			$(ns \leftarrow 25a')$		
8.178	1.98	4s	8.707	1.98	4s	8.920	1.97	4s
10.00(7)(s,w)	2.00	5s	–	–	–	–	–	–
10.66(5)(w)	2.01	6s	–	–	–	–	–	–
$(np \leftarrow 4a'')$			$(np \leftarrow 26a')$			$(np \leftarrow 25a')$		
9.04(7)(b)	1.65	4p	9.61(5)(b)	1.63	4p	–	–	–
10.30(2)(s)	1.66	5p	–	–	–	–	–	–
$(np' \leftarrow 4a'')$			$(np' \leftarrow 26a')$			$(np' \leftarrow 25a')$		
9.39(6)(s,w)	1.47	4p'	9.90(0)(s)	1.48	4p'	–	–	–
10.41(5)(s)	1.49	5p'	–	–	–	–	–	–
$(nd \leftarrow 4a'')$			$(nd \leftarrow 26a')$			$(nd \leftarrow 25a')$		
–	–	3d	10.41(5)(s)	0.11	3d	–	–	–
10.60(6)(s,w)	0.14	4d	–	–	–	–	–	–
$(nd' \leftarrow 4a'')$			$(nd' \leftarrow 26a')$			$(nd' \leftarrow 25a')$		
9.95(9)(s,w)	0.05	3d'	10.45(4)(s,w)	0.07	3d'	10.66(5)(w)	0.05	3d'
10.66(5)(w)	0.01	4d'	–	–	–	–	–	–
$IE_7 = 12.70$ eV $(3a'')^{-1}$			**$IE_8 = 13.54$ eV** $(24a')^{-1}$			**$IE_9 = 13.81$ eV** $(23a')^{-1}$		
$(ns \leftarrow 3a'')$			$(ns \leftarrow 24a')$			$(ns \leftarrow 23a')$		
9.51(5)(s)	1.93	4s	10.23(4)(s,b)	1.97	4s	10.41(5)(s)	2.00	4s
$(np \leftarrow 3a'')$								
10.23(4)(s,b)	1.65	4p	–	–	–	–	–	–
$(np' \leftarrow 3a'')$								
10.60(6)(s,w)	1.45	4p'	–	–	–	–	–	–

[a](b) broad structure; (w) weak feature; (s) shoulder structure (the last decimal of the energy value is given in brackets for these less-resolved features);

stretching, $\nu'_{21}(a')$ (in a_0 units), are shown in Fig. 6. These were calculated at the TD-DFT/B3LYP/aug-cc-pVDZ level of theory in the C_1 symmetry group while allowing all atoms to relax following the respective mode. Although unambiguous assignments of the absorption features were not possible for the almost degenerate C–H in-plane bending modes, $\nu'_{16}(a')$ and $\nu'_{17}(a')$, with ground state energies of 0.144 and 0.140 eV (1158 and1129 cm^{-1}), for the present discussion on the nuclear dynamics governing the nature of those electronic states, we show $\nu'_{17}(a')$ only.

Fig. 6 shows that all states have bound characters within the three reaction coordinates. The second singlet-singlet electronic transition in the photoabsorption spectrum assigned to $2\pi^*(7a'')\leftarrow\pi/n_{Cl}(6a'') + 1\pi^*(7a'')\leftarrow\pi/n_{Cl}(6a'') + 1\pi^*(7a'')\leftarrow\pi/n_{Cl}(5a'')$, $(3\ ^1A'\leftarrow\widetilde{X}\ ^1A')$ shows some quanta mainly due to C=C stretching, $\nu'_7(a')$, C–H in-plane bending, $\nu'_{16}(a')/\nu'_{17}(a')$, and C–Cl stretching, $\nu'_{21}(a')$ modes (Table 3). This is in agreement with the structure mostly noted in the 5.4–6.8 eV energy region of the VUV photoabsorption spectrum (Fig. 3). Moreover, the PECs exhibit some avoided crossings for the majority of the computed states. This may imply that in the adiabatic description, as the

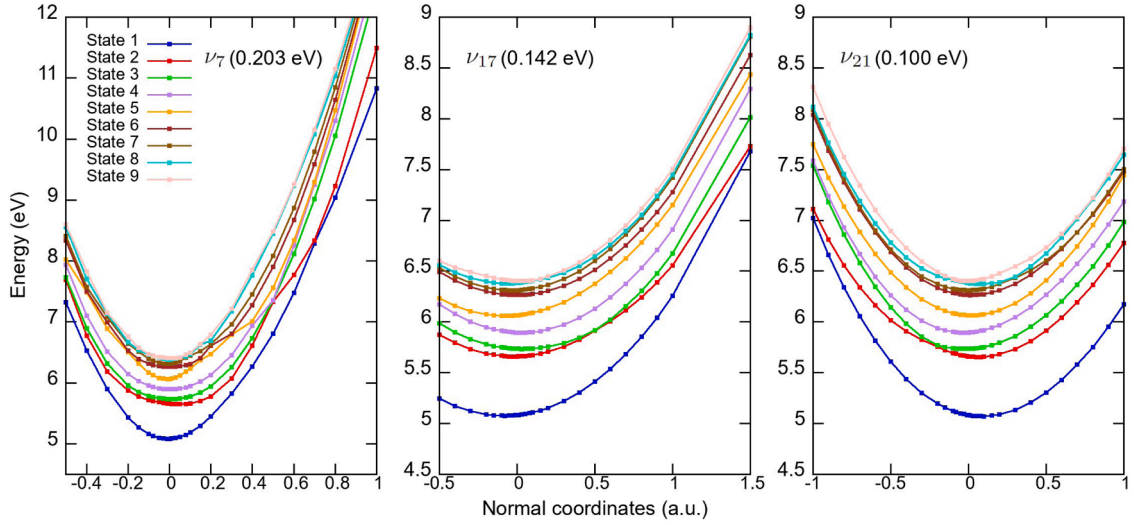

Fig. 6. PECs for the nine lowest-lying singlet excited states of 2-chlorotoluene following the C=C stretching, $\nu'_7(a')$, C–H in-plane bending, $\nu'_{17}(a')$, and C–Cl stretching, $\nu'_{21}(a')$ modes (in a_0 units). The calculations were performed at the TD-DFT/B3LYP/aug-cc-pVDZ level of theory in the C_1 symmetry group. See text for details.

displacement along each vibrational mode is changed, a change from in the initial character to the final character is achieved. In order to check this assumption, we have also plotted in Figures S5–S7 the character of some of the electronic transitions from the ground state to each state, together with their major contributions, at different interatomic displacements. As far as C=C stretching, $\nu'_7(a')$ is concerned, we also show three different snapshots in Fig. S5 (a)–(c).

The second excited electronic state is shown in Fig. 6 by a red colour as "State 2″. The avoided crossings are at ~ 0.5 a_0 for C=C stretching, $\nu'_7(a')$ and C–H in-plane bending, $\nu'_{17}(a')$, modes while at ~ -0.25 a_0 for C–Cl stretching, $\nu'_{21}(a')$ mode. In Figs. S5 (a)–(c) the state is kept π* across the entire displacement range, although from different LUMOs, thus rendering valence character for the vibronic transition along the C=C stretching, $\nu'_7(a')$ mode. However, for the C–H in-plane bending, $\nu'_{17}(a')$ mode in Fig. S6, as the avoided crossing is reached, the initial π* antibonding character changes to Rydberg, which is clearly visible at a geometry of +0.6 a_0 (Fig. S6). It is also interesting to note that internal conversion from initial Rydberg to valence character is noted for the PEC along the C–Cl bond (Fig. S7) at no change of the normal coordinate. While compressing the bond at a geometry of -0.7 a_0 the Rydberg nature of the MO prevails, in the interatomic equilibrium distance, the valence character is attained. This is certainly expected given the relevance of the σ* antibonding character yielding C–Cl bond excision, in good agreement with the calculated transition energy of 6.403 eV with an oscillator strength of ~0.0011 and assigned to $\sigma^*_{CCl}(31a')\leftarrow\pi/n_{Cl}(6a'')$, $(6\,{}^1A''\leftarrow\widetilde{X}\,{}^1A')$ in Table S1.

The higher energy states (labelled in Fig. 6 as 6, 7, 8 and 9) are almost degenerate at the equilibrium distances, which is not surprising given that they originate from the same MOs, i.e., either the HOMO (n_{Cl}/π, 6a″) or the HOMO-1 ($\pi_{C=C}/n_{Cl}$, 5a″). However, states 5 and 6, at energies > 6.5 eV, cross slightly above the equilibrium internuclear distance. Such behaviour may result in a relevant adiabatic character, which is responsible for the internal conversion either from valence to Rydberg or vice-versa in the asymptotic limit, as relative displacements $\Delta R_{C=C}$ and ΔR_{C-Cl} are stretched away from their equilibrium distance. We also note that the higher-lying energy states labelled 7, 8 and 9 cross close to the $\Delta R_{C=C}$ equilibrium distance where avoided crossings in the Franck-Condon region can take the system through states which lead to a valence character along the C=C stretching bond. The different avoided crossings may indicate conical intersections in the full multidimensional landscape, that will be worth investigating but are not within the scope of the present work.

5.6. *Absolute photoabsorption cross sections and atmospheric photolysis*

We report the absolute ultra-violet photoabsorption cross-sections of 2-chlorotoluene in the photon energy region 4.0–10.8 eV, with Table 1 listing the major electronic transitions and their values in units of Mb. Previous study of the vacuum ultraviolet photoabsorption has covered the wavelength region 172.2 to 279.1 nm (4.4 to 7.2 eV) [20], and is found to be in reasonable agreement with the present cross-sections in magnitude at 4.679 eV (265 nm) and 6.078 eV (204 nm). However, Shama [20] reports the highest cross-section value of ~ 230 Mb at ~6.5 eV (190 nm) which is 17 % higher than our value of 195.83 Mb.

From the absolute photoabsorption cross-section values in combination with the NASA solar actinic flux data [33], we can estimate the atmospheric photolysis of 2-chlorotoluene from 0 km altitude up to the limit of the stratopause (50 km altitude). We have reported this methodology before and details of it can be found from the work of Limão-Vieira and co-workers [34]. The quantum yield for dissociation is assumed to be 1.0 for C–Cl bond excision, although the single available photodissociation work of Gu *et al.* [12] gives no indication about such value. Photolysis lifetimes of less than 1 sunlit day were calculated at altitudes above 23 km. However, at lower altitudes (< 20 km) the photolysis lifetimes of 2-chlorotoluene can reach several tens of sunlit days. Mohan et al. [16] and Merga et al. [15] reported gas-phase kinetics studies for 2-chlorotoluene reactions with the ·OH radical, with a rate value of $k_{OH} = 1.54 \times 10^{-13}$ cm^3 molecule^{-1} s^{-1}. According to Mohan et al. [16], the OH radical is expected to react mainly by addition to the benzene ring. However, it has to be proven if this type of reaction may provide the main sink mechanism in the Earth's atmosphere. Notwithstanding, our results show that UV photolysis can be a relevant removal mechanism of any 2-chlorotoluene in the stratosphere.

6. Conclusions

We have obtained a photoabsorption spectrum of 2-chlorotoluene in the energy range 4.0–10.8 eV (310–115 nm). The absorption features have been assigned to valence, mixed valence-Rydberg and Rydberg transitions with the aid of quantum chemical calculations, on the vertical excitation energies and oscillator strengths. The major fine structure in the spectrum has been assigned to excitation of C–H stretching (CH_3), $\nu'_6(a')$, C–H in-plane bending, $\nu'_{16}(a')/\nu'_{17}(a')$, C–Cl stretching

(C–CH_3 stretching and C–C in-plane bending), $\nu'_{21}(a')$ and C–C in-plane bending $\nu'_{23}(a')$ modes.

The absolute photoabsorption cross-sections have also been used to estimate photolysis rates in the Earth's atmosphere from sea-level up to the limit of the stratosphere (50 km altitude), indicating that solar photolysis is expected to be a key sink mechanism at altitudes higher than 23 km. Time dependent density functional theory with aug-cc-pVDZ basis set has been used to calculate potential energy curves for the nine lowest-lying singlet excited states of 2-chlorotoluene following the C=C stretching, $\nu'_7(a')$, C–H in-plane bending, $\nu'_{17}(a')$, and C–Cl stretching, $\nu'_{21}(a')$ modes. The results show relevant excited state dynamics along the potential energy curves of each vibrational mode, with important avoided crossings responsible for internal conversion from initial Rydberg states to final valence character and vice-versa.

CRediT authorship contribution statement

P.A.S. Randi: Software, Investigation, Data curation. **S. Kumar:** Visualization, Investigation, Data curation. **A. Souza Barbosa:** Validation, Software. **U.S. Akther:** Visualization, Methodology. **N.C. Jones:** Writing – review & editing, Writing – original draft, Validation, Supervision, Methodology, Investigation, Formal analysis, Data curation. **S.V. Hoffmann:** Writing – review & editing, Writing – original draft, Supervision, Resources, Project administration, Methodology, Funding acquisition, Formal analysis, Data curation. **M.H.F. Bettega:** Writing – review & editing, Validation, Supervision, Software, Formal analysis, Data curation. **P. Limão-Vieira:** Writing – review & editing, Writing – original draft, Supervision, Funding acquisition, Formal analysis.

Declaration of competing interest

The authors declare that they have no known competing financial interests or personal relationships that could have appeared to influence the work reported in this paper.

Acknowledgments

PASR acknowledges support from the Brazilian agency Coordenação de Aperfeiçoamento de Pessoal de Nível Superior (CAPES). ASB and MHFB acknowledge support from the Brazilian agency Conselho Nacional de Desenvolvimento Científico e Tecnológico (CNPq). PASR, ASB and MHFB also acknowledge Prof. Carlos de Carvalho for computational support at LFTC-DFis-UFPR and at LCPAD-UFPR. The authors wish to acknowledge the beam time at the ISA synchrotron, Aarhus University, Denmark. The research leading to this result has been supported by the project CALIPSOplus under Grant Agreement 730872 from the EU Framework Programme for Research and Innovation HORIZON 2020. PLV acknowledges the Portuguese National Funding Agency (FCT) through research grant CEFITEC (UIDB/00068/2020), his visiting professor position at Federal University of Paraná, Curitiba, Brazil and CAPES PrInt/UFPR. This work was also supported by Radiation Biology and Biophysics Doctoral Training Programme (RaBBiT, PD/00193/2012) and UCIBIO (UIDB/04378/2020).

Supplementary materials

Supplementary material associated with this article can be found, in the online version, at doi:10.1016/j.molstruc.2024.141045.

Data availability

Data presented in this publication are available upon request to the authors.

References

[1] I. Martí, R. Lloret, J. Martín-Alonso, F. Ventura, Determination of chlorinated toluenes in raw and treated water samples from the Llobregat river by closed loop stripping analysis and gas chromatography-mass spectrometry detection, J. Chromatogr. A. 1077 (2005) 68–73, https://doi.org/10.1016/j.chroma.2005.04.051.

[2] D. Dobslaw, K.H. Engesser, Biodegradation of gaseous emissions of 2-chlorotoluene by strains of Rhodococcus sp. in polyurethane foam packed biotrickling filters, Sci. Total Environ. 639 (2018) 1491–1500, https://doi.org/10.1016/j.scitotenv.2018.05.278.

[3] L. Li, D. Zhang, W. Hu, Y. Yang, S. Zhang, R. Yuan, P. Lv, W. Zhang, Y. Zhang, Y. Zhang, Improving VOC control strategies in industrial parks based on emission behavior, environmental effects, and health risks: A case study through atmospheric measurement and emission inventory, Sci. Total Environ. 865 (2023) 161235, https://doi.org/10.1016/j.scitotenv.2022.161235.

[4] C. Serralheiro, D. Duflot, F.F. Silva, S.V. Hoffmann, N.C. Jones, N.J. Mason, B. Mendes, P. Limão-Vieira, Toluene valence and rydberg excitations as studied by ab initio calculations and vacuum ultraviolet (VUV) synchrotron radiation, J. Phys. Chem. A. 119 (2015) 9059–9069.

[5] P.A.S. Randi, S. Kumar, A.I. Lozano, M.H.F. Bettega, S.V Hoffmann, N.C. Jones, A. S. Barbosa, Limão-vieira, valence and rydberg excitations of 2-fluorotoluene in the 4.4–10.8 eV photoabsorption energy region, J. Quant. Spectrosc. Radiat. Transf. 303 (2023) 108597.

[6] L.V.S. Dalagnol, S. Kumar, A.I. Lozano, M.H.F. Bettega, N.C. Jones, S.V. Hoffmann, A.S. Barbosa, P. Limão-Vieira, Valence and Rydberg excitations of 4-fluorotoluene in the 4.3–10.8 eV photoabsorption energy region, J. Quant. Spectrosc. Radiat. Transf. 327 (2024) 109125, https://doi.org/10.1016/j.jqsrt.2024.109125.

[7] E. Bandeira, S. Kumar, A.I. Lozano, M.H.F. Bettega, S.V. Hoffmann, N.C. Jones, A. S. Barbosa, P. Limão-Vieira, Valence and Rydberg excitations of 3-fluorotoluene in the 4.4–10.8 eV photoabsorption energy region, J. Quant. Spectrosc. Radiat. Transf. 312 (2024) 108796.

[8] A.S. Barbosa, F.F. Silva, A. Rebelo, S.V. Hoffmann, M.H.F. Bettega, P. Limão-Vieira, Valence and Rydberg excitations of 2,4- and 2,6-difluorotoluene as studied by vacuum ultraviolet synchrotron radiation and ab initio calculations, J. Phys. Chem. A. 120 (2016) 8998–9007.

[9] N.J. Mason, A. Dawes, R. Mukerji, E.A. Drage, E. Vasekova, S.M. Webb, P. Limão-Vieira, Atmospheric chemistry with synchrotron radiation, J. Phys. B At. Mol. Opt. Phys. 38 (2005) S893–S911, https://doi.org/10.1088/0953-4075/38/9/027.

[10] S. Fujisawa, I. Oonishi, S. Masuda, K. Ohno, Y. Harada, Penning ionization electron spectroscopy of dichlorobenzenes, J. Phys. Chem. 95 (1991) 5742–5749, https://doi.org/10.1021/j100164a017.

[11] N. Kishimoto, M. Matsumoto, E. Matsumura, K. Ohno, Collision-energy-resolved Penning ionization electron spectroscopy of toluene and chlorotoluenes: Stereodynamics in collisional ionization and anisotropic interactions with He* (23S) atoms, Eur. Phys. J. D. 38 (2006) 75–84, https://doi.org/10.1140/epjd/e2005-00269-3.

[12] X.Bin Gu, G.J. Wang, J.H. Huang, K.L. Han, G.Z. He, N.Q. Lou, Substitution effects of methyl: Photodissociation of m-, o- and p-chlorotoluene at 266 nm, Phys. Chem. Chem. Phys. 4 (2002) 6027–6033, https://doi.org/10.1039/b205228h.

[13] M. Govindarajan, K. Ganasan, S. Periandy, M. Karabacak, S. Mohan, Vibrational spectroscopic analysis of 2-chlorotoluene and 2-bromotoluene: A combined experimental and theoretical study, Spectrochim. Acta, Part A. 77 (2010) 1005–1013, https://doi.org/10.1016/j.saa.2010.08.038.

[14] J. Wang, M. Ren, S. Wang, Y. Qu, Molecular structure and vibrational spectra of o-chlorotoluene, m-chlorotoluene, and p-chlorotoluene by ab initio HF and DFT calculations, Spectrochim. Acta, Part A. 78 (2011) 1126–1132, https://doi.org/10.1016/j.saa.2010.12.064.

[15] G. Merga, B.S.M. Rao, H. Mohan, J.P. Mittal, Reactions of OH and SO4•- with some halobenzenes and halotoluenes: A radiation chemical study, J. Phys. Chem. 98 (1994) 9158–9164, https://doi.org/10.1021/j100088a012.

[16] H. Mohan, M. Raob, J.P. Mittal, Studies on StructureReactivity in the Reaction of OH Radicals with Substituted Halobenzenes in Aqueous Solutions, J. Chem. Soc., Faraday Trans. 2 (1991) 1387–1392.

[17] E.C. Richard, R.A. Walker, J.C. Weisshaar, Hindered internal rotation and torsion-vibrational coupling in ortho-chlorotoluene (S1) and ortho-chlorotoluene+ (D0), J. Chem. Phys. 104 (1996) 4451–4469, https://doi.org/10.1063/1.471198.

[18] D. Gerhard, A. Hellweg, I. Merke, W. Stahl, M. Baudelet, D. Petitprez, G. Wlodarczak, Internal rotation and chlorine nuclear quadrupole coupling of o-chlorotoluene studied by microwave spectroscopy and ab initio calculations, J. Mol. Spectrosc. 220 (2003) 234–241, https://doi.org/10.1016/S0022-2852(03)00125-5.

[19] H. Keller-Rudek, G.K. Moortgat, R. Sander, R. Sörensen, The MPI-Mainz UV/VIS spectral atlas of gaseous molecules of atmospheric interest, Zagazig University, 2013.

[20] S.A.A.E.A. Shama, Vacuum ultraviolet absorption spectra of organic compounds in gaseous and liquid state, Zagazig University, Egypt, 1991.

[21] S. Eden, P. Limão-Vieira, S.V. Hoffmann, N.J. Mason, VUV photoabsorption in CF3X (X = Cl, Br, I) fluoro-alkanes, Chem. Phys. 323 (2006) 313–333.

[22] M.H. Palmer, T. Ridley, S.V. Hoffmann, N.C. Jones, M. Coreno, M. De Simone, C. Grazioli, M. Biczysko, A. Baiardi, P. Limão-Vieira, Interpretation of the vacuum ultraviolet photoabsorption spectrum of iodobenzene by ab initio computations, J. Chem. Phys. 142 (2015) 134302.

[23] R. Bauernschmitt, R. Ahlrichs, Treatment of electronic excitations within the adiabatic approximation of time dependent density functional theory, Chem. Phys. Lett. 256 (1996) 454–464.

[24] M.E. Casida, Time-dependent density-functional theory for molecules and molecular solids, J. Mol. Struct.Theochem. 914 (2009) 3–18.
[25] A.D. Beck, Density-functional thermochemistry. III. The role of exact exchange, J. Chem. Phys. 98 (1993) 5648–5652.
[26] C. Lee, W. Yang, R.G. Parr, Development of the Colle-Salvetti correlation-energy formula into a functional of the electron density, Phys. Rev. B. 37 (1988) 785–789.
[27] G.M.J. Barca, C. Bertoni, L. Carrington, D. Datta, N. De Silva, J.E. Deustua, D. G. Fedorov, J.R. Gour, A.O. Gunina, E. Guidez, T. Harville, S. Irle, J. Ivanic, K. Kowalski, S.S. Leang, H. Li, W. Li, J.J. Lutz, I. Magoulas, J. Mato, V. Mironov, H. Nakata, B.Q. Pham, P. Piecuch, D. Poole, S.R. Pruitt, A.P. Rendell, L.B. Roskop, K. Ruedenberg, T. Sattasathuchana, M.W. Schmidt, J. Shen, L. Slipchenko, M. Sosonkina, V. Sundriyal, A. Tiwari, J.L. Galvez Vallejo, B. Westheimer, M. Włoch, P. Xu, F. Zahariev, M.S. Gordon, Recent developments in the general atomic and molecular electronic structure system, J. Chem. Phys. 152 (2020) 154102.
[28] K. Emrich, An extension of the coupled cluster formalism to excited states (I), Nucl. Phys. A 351 (1981) 379–396.
[29] H. Sekino, R.J. Bartlett, A linear response, coupled-cluster theory for excitation energy, Int. J. Quantum Chem. 26 (1984) 255–265.
[30] J.F. Stanton, R.J. Bartlett, The equation of motion coupled-cluster method. A systematic biorthogonal approach to molecular excitation energies, transition probabilities, and excited state properties, J. Chem. Phys. 98 (1993) 7029–7039.
[31] R.J. Bartlett, Coupled-cluster theory and its equation-of-motion extensions, Wiley Interdiscip. Rev. Comput. Mol. Sci. 2 (2012) 126–138.
[32] R.M. Parrish, L.A. Burns, D.G.A. Smith, A.C. Simmonett, A.E. DePrince, E. G. Hohenstein, U. Bozkaya, A.Y. Sokolov, R. Di Remigio, R.M. Richard, J. F. Gonthier, A.M. James, H.R. McAlexander, A. Kumar, M. Saitow, X. Wang, B. P. Pritchard, P. Verma, H.F. Schaefer, K. Patkowski, R.A. King, E.F. Valeev, F. A. Evangelista, J.M. Turney, T.D. Crawford, C.D. Sherrill, Psi4 1.1: An open-source electronic structure program emphasizing automation, advanced libraries, and interoperability, J. Chem. Theory Comput. 13 (2017) 3185–3197.
[33] Chemical kinetics and photochemical data for use in stratospheric modelling, evaluation number 12, NASA, jet propulsion laboratory, JPL (1997). Publication 97-4, January 15.
[34] P. Limão-Vieira, S. Eden, P.A. Kendall, N.J. Mason, S.V. Hoffmann, VUV photo-absorption cross-section for CCl2F2, Chem. Phys. Lett. 364 (2002) 535–541.